

Towards a Stopping Rule for the OSEM Algorithm for Iterative Image Reconstruction in PET

Anastasios Gaitanis, George Kontaxakis, *Senior Member, IEEE*, George Spyrou, George Panayiotakis, and George Tzanakos, *Senior Member, IEEE*

Abstract— We have studied certain properties of the OSEM algorithm for iterative image reconstruction in PET. This work is within the framework of our principal objective that is the development and evaluation of a stopping criterion for this iterative algorithm. To investigate the problem of the deterioration of the image quality after several iterations, the statistical properties of the pixel updating coefficients have been studied. Preliminary results show that the values of these coefficients for the pixels that correspond to areas in the source with non-zero activity distribution form a histogram composed of a peak region around to 1.0 and a tail below this value. Given the different rate of convergence of the pixel values within an image, this tail distribution corresponds to those pixels that are yet far from reaching their corresponding true values. We demonstrate that the minimum value of the tail distribution is directly related to the quality of the reconstructed images. The possibility of exploring this observation in order to formulate a stopping criterion for the OSEM algorithm is discussed.

I. INTRODUCTION

Positron Emission Tomography (PET) imaging is presently used in a wide area of medical disciplines, such as oncology, neurology, etc. The proper selection of the image reconstruction algorithm for a particular study has a significant impact on the quality of the images produced by a PET camera [1]. Modern PET scanners employ iterative image reconstruction algorithms such as the maximum-likelihood expectation-maximization (MLEM) [2] and the ordered subsets expectation-maximization (OSEM) [3] algorithms as well as several of their variants [4]. Since the images produced by the OSEM algorithm have been observed to become noisier as iterations proceed, something that might have negative impact on the diagnostic quality

offered by these images, a robust stopping criterion is essential to guarantee the stopping of the iterative process when the reconstructed image provides optimal signal-to-noise properties.

Several research groups in the past have proposed stopping rules for the MLEM algorithm [5]-[8]. In this work we have been looking for a stopping rule of the OSEM algorithm that would be independent of the characteristics of the object under study. To the best of our knowledge, no known study has addressed the issue of a stopping rule for the OSEM algorithm. This work extends the methodology and results obtained in previous work carried out by our group [7]-[9] for the case of the MLEM iterative image reconstruction algorithm for PET.

II. MATERIALS AND METHODS

A. OSEM algorithm

The OSEM algorithm is an accelerated implementation of the MLEM algorithm. In this case the projection data are grouped into ordered subsets (OS). The EM algorithm is then applied successively to each of these subsets. The image obtained from this process on one subset is the initial image for the next one, etc. It has been observed that the image produced after one iteration of the OSEM algorithm over n subsets is very similar to the image obtained after n iterations of the MLEM algorithm over the complete data set of projections.

The mathematical expression of the pixel updating process in the OSEM algorithm is [3]:

$$x_i^{(k)} = x_i^{(k-1)} C_i^{(k-1)} \quad (1)$$

$$C_i^{(k-1)} = \frac{1}{\sum_{j \in S_n} a_{ij}} \sum_{j \in S_n} \frac{a_{ij} y_j}{\sum_{i=1} x_i^{(k-1)} a_{ij}} \quad (2)$$

where i is the i th pixel in the image vector, $\mathbf{x}^{(k)}$ is the image vector obtained at the k th iteration, $\mathbf{C}^{(k-1)}$ is the vector of the pixel updating coefficients at the $(k-1)$ th iteration, S_n is the set of n subsets, y_j is the projected data in j th line-of-response (LOR) and a_{ij} represents the probability that an annihilation event generated in the area of the i th pixel is detected in the j th LOR. All a_{ij} values form a matrix, that is also known as the system matrix for a given scanner configuration.

Manuscript received November 14, 2008.

A. Gaitanis is with the Department of Medical Physics, Medical School, University of Patras and Biomedical Research Foundation of Athens Academy, Soranou Efessiou 4, 11527 Greece (e-mail: agaitanis@bioacademy.gr).

G. Kontaxakis is with the Universidad Politécnica de Madrid, E.T.S.I. Telecomunicación, Dpto. Ingeniería Electrónica, 28040 Madrid, Spain (e-mail: gkont@die.upm.es).

G. Spyrou is with the Biomedical Research Foundation of Athens Academy, Soranou Efessiou 4, 11527 Greece (e-mail: gspyrou@bioacademy.gr).

G. Panayiotakis is with the Department of Medical Physics, Medical School, University of Patras, 26500 Patras, Greece (e-mail: panayiot@upatras.gr).

G. Tzanakos is with the University of Athens, Department of Physics, Division of Nuclear & Particle Physics, Panepistimioupoli, Zografou, Athens 15771, Greece (e-mail: tzanakos@phys.uoa.gr).

B. The PET scanner

We have modeled a single-ring PET camera with 128 scintillation crystals on the ring, a detector width of 7.36 mm and a field of view (FOV) of 200×200 mm². The detector ring radius is 150 mm. The total number of LOR is 8128. Image grids with a size of 128×128 (pixel side = 1.56 mm) have been employed. Monte Carlo methods have been used for the simulation of the activity distribution in the source, the generation of positron-electron annihilations, the production of gamma-rays, their propagation in the source and their detection by the scintillation detectors. Ideal conditions have been assumed (100% detector efficiency, no Compton scattering or photoelectric effects in the source and the detectors, no random coincidences, etc).

C. The system matrix

The system matrix depends on the geometry and configuration of the PET scanner (image grid and scanner's layout). In this work, the system matrix for the camera configuration employed has been calculated using Monte Carlo methods. In the area that corresponds to each pixel i a sufficient number of events N_{tot} are generated and the simulated gamma-rays are recorded in each line-of-response. The probability value α_{ij} is then given by the expression:

$$\alpha_{ij} = \frac{N_j}{N_{tot}} \quad (3)$$

where N_j is the number of those events detected within the j th LOR. The accuracy of this method depends on the total number of annihilation events generated in each pixel. For this reason 10^7 gamma-rays have been uniformly generated in each pixel. In that way the relative error is less than 1%.

D. Data generation

For this study the digital Hoffman brain phantom [10] has been used. This phantom consists of 18 2-dimensional image slices. The pixel values in each slice correspond to the activity distribution in the area covered by each pixel in the source. A proportional number of gamma rays have been generated using Monte Carlo methods for this pixel and their trajectories have been followed until they hit a detector on the camera's ring. For each slice various activity distributions have been simulated, ranging from 200k to 6.0M counts.

Using this procedure, data from the 18 Hoffman brain phantom slices have been acquired at different activity distribution levels and have been reconstructed using the OSEM algorithm. Two and four subsets have been employed.

For the validation of the results obtained, we have used data acquired based on the Digimouse phantom [11] and according to a similar procedure as the one followed with

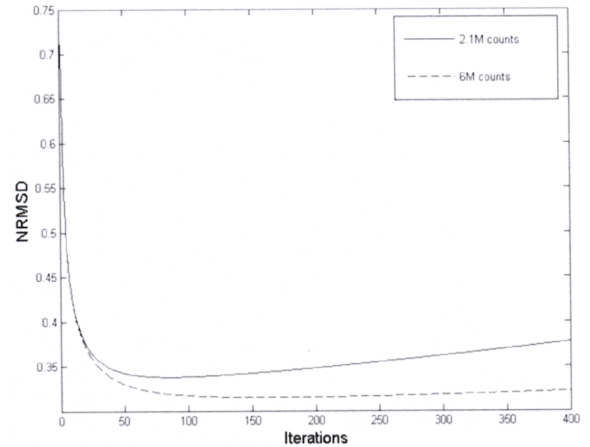


Fig. 1. The NRMSD curve for the Hoffman brain phantom slice #9 (2.1 and 6M counts, OSEM with 2 subsets). Images with higher activity levels produces images with lower levels of noise added along the iterative process. (Lower values of NRMSD).

the Hoffman brain phantom: based on the activity distribution in the Digimouse image slices, a certain number of counts has been generated, assuming an ideal, noise-free case. These data have been then reconstructed using the OSEM algorithm. The stopping criterion developed based on the Hoffman brain phantom has been validated using the data reconstructed from the Digimouse phantom.

E. Image quality estimators

In the OSEM algorithm an initial estimate image $\mathbf{x}^{(0)}$ (typically a uniform activity distribution for all pixels) is used as starting point. The quality of the reconstructed image steadily improves during the first iterations however after a certain point in the iterative process the image quality deteriorates due to noise. As a quantitative measure for the image quality, the Normalized Root Mean Square Deviation (NRMSD) [9] is employed as figure of merit (FOM):

$$\text{NRMSD}(k) = \sqrt{\frac{\sum_{i=1}^I (x_i^{(k)} - \hat{x}_i)^2}{\sum_{i=1}^I \hat{x}_i^2}} \quad (4)$$

where $\hat{\mathbf{x}}$ and $\mathbf{x}^{(k)}$ are the phantom image and the reconstructed image at a given iteration k respectively.

III. RESULTS

Fig. 1 shows an example of the behavior of the NRMSD. As it can be observed, there is an improvement of the image quality during the initial iterations (NRMSD value decreases), and a minimum is reached at the iteration in which the image quality is closest to the phantom image. After this point, the image quality begins to deteriorate. An example of this is shown on Fig. 2. The Hoffman phantom slice #9 is reconstructed using OSEM with 2

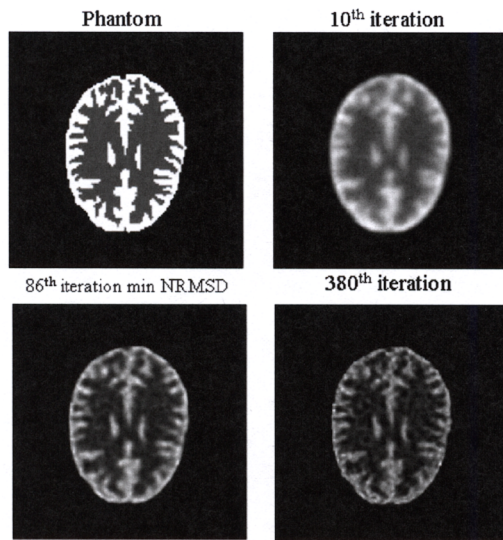


Fig. 2. The Hoffman brain phantom slice #9 for 2.1M simulated counts. As it is shown there is an improvement of image quality from the beginning (10th iteration) to the iteration where minimum NRMSD occurs (86th iteration) and after that, the deterioration phase begins (380th iteration).

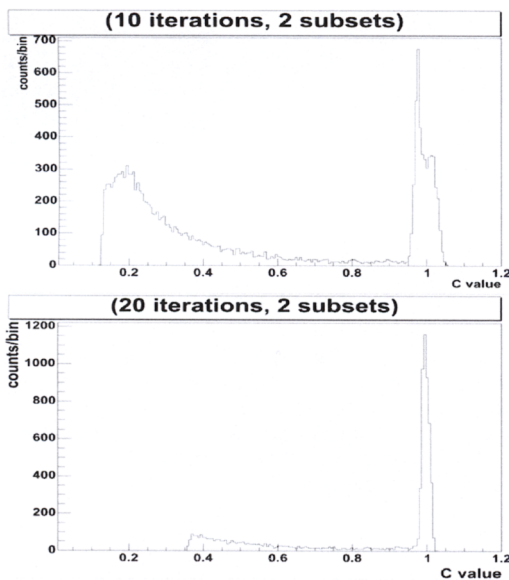


Fig. 3. Histograms show the distribution of the values of the updating coefficients C . Each histogram has two components: a) one component around 1.0 corresponds to those pixels for which reconstruction has been completed and b) a tail, namely a region of values lower than 1.0 corresponds to pixels which have not yet reached convergence. For these histograms the reconstruction was performed using two subsets.

subsets. The reconstructed image is shown after 10, 86 (iteration which NRMSD gets its minimum value) and 380 iterations respectively.

From equation (1) it is clear that the evolution of the values of the coefficients C represents the convergence rate

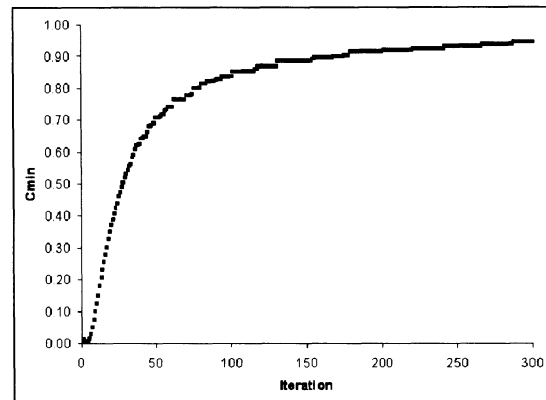


Fig. 4. C_{min} as a function of the iterations of Hoffman slice #9. 6M counts have been simulated.

for a particular image. Motivated by this observation we have studied further the statistical behavior of C for all non-zero pixels of the reconstructed image versus the number of iterations. Fig. 3 shows the histograms of the coefficients C for the Hoffman brain phantom slice #9 at the 10th and 20th OSEM iteration. The minimum value of the histogram (C_{min}) moves to higher values as the iteration goes on. We define a variable $C_{min} = \min \{C_i, i=1,2,\dots, I\}$, where I is the total number of pixels with non-zero activity distribution levels in the image.

In other words C_{min} is the minimum value of the coefficients vector C for the non-zero pixels in the reconstructed image at the current iteration. In this work the dependence of C_{min} of the iteration number and its relationship to the minimum NRMSD value will be investigated. In previous work [9] we have shown that C_{min} increases monotonically with iteration number in the case of MLEM algorithm. A similar behavior has been observed in the case of OSEM algorithm (Fig. 4).

The NRMSD is used for the comparison between the reconstructed and phantom (initial) image. The minimum NRMSD value corresponds to the smallest possible difference between these two images according to equation (4). At the iteration when the minimum NRMSD value is reached, the C_{min} value has been recorded. This has been repeated for all slices in the Hoffman brain phantom. Following this, the C_{min} values have been averaged over all slices and the *mean* C_{min} values have been calculated. Fig 5 shows the *mean* C_{min} values against the activity distribution for 2 and 4 subsets. This figure shows that *mean* C_{min} values increase monotonically as a function of the activity distribution levels, with similar shapes for both curves. In the case of image reconstruction with OSEM with 2 subsets these values are higher than them produced by OSEM with 4 subsets. This means that the number of subsets affects the reconstruction process, something that correlates well with the results shown in Fig. 1, in which it is shown that the

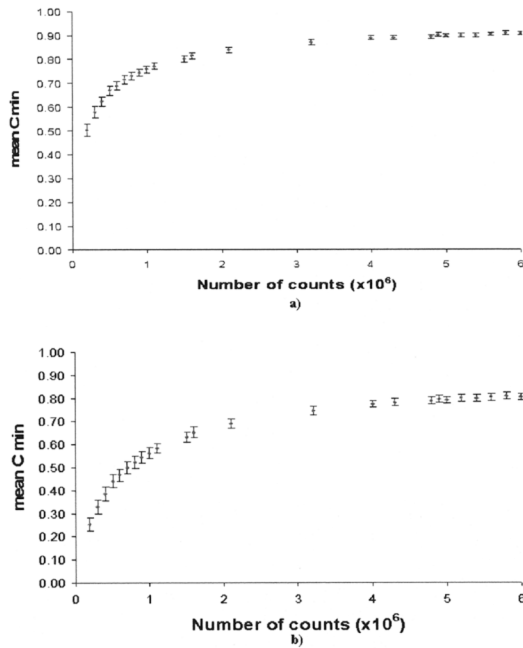


Fig. 5. Mean C_{min} values versus number of counts a) for 2 subsets and b) for 4 subsets

minimum value of the NRMSD (a FOM that in general can be used only in case of simulation studies or phantom acquisitions with known activity distribution in the source) is reached at higher iteration numbers as the number of counts increases.

In order to parameterize quantitatively the dependence of C_{min} on the number of counts, we have fitted the plots shown in Fig. 5. A fitting method has been applied using the weighted average and associated errors of *mean* C_{min} .

Different equation forms have been tested such as linear, polynomial or Gaussian equations; however the most efficient (according to the R^2 value produced by each fitting) had the following rational form:

$$K = A \frac{N + \alpha}{N + b} \quad (5)$$

where N is the number of counts in the image, expressed in millions. In that way, the behavior of mean C_{min} has been expressed as a function of the number of counts N in the image, a parameter known in all cases, including real PET scans. The parameters A , a and b have been specified and as it is shown in Table I are different, depending on each set of subsets.

A. Proposed Stopping Rule of the OSEM algorithm

From the above analysis it appears that a stopping rule could be formulated based on the variable K namely from the known total number of acquired counts, the value of K

	A	a	b
2 subsets	0.943 ± 0.006	0.103 ± 0.021	0.362 ± 0.037
4 subsets	0.884 ± 0.008	0.041 ± 0.016	0.618 ± 0.045

TABLE I
PARAMETERS A , a AND b OF FITTING EQUATION FOR EACH SUBSETS

can be calculated using equation (5) and the OSEM algorithm can be stopped at the iteration when the C_{min} value is equal or higher to value K . In other words the proposed stopping rule for OSEM can be expressed using pseudo-code as:

```

for each iteration
  if  $C_{min} = \min\{C_i\} \geq K$ 
  then
    stop the reconstruction
  end

```

IV. DISCUSSION AND CONCLUDING REMARKS

A. Validation of the Stopping Rule

For the validation of the proposed stopping rule a different set of images were used as phantoms. This set of real scanned images originated from the Digimouse phantom [11]. Using slices from Digimouse as input, the projection data were generated. The number of counts in each image slice was known and using the equation (5) the values of K were estimated. The OSEM algorithm for 2 and 4 subsets stopped when the stopping condition was met. Here, we present the results regarding the slices #16, #33 and #106. The number of counts in each slice was 2.68, 1.25 and 6.51M counts respectively. In the case of 2 subsets, the algorithm stopped after 123, 69 and 173 iterations respectively, while in the case of 4 subsets the algorithm stopped after 60, 32 and 81 iterations respectively. In Fig. 6 the phantom, the reconstructed image and the difference for each slice are shown. The difference images between the phantom and reconstructed show that the images produced using the proposed stopping rule are almost the same, suggesting that the reconstruction algorithm works quite well.

B. Conclusions

Summarizing, these preliminary results show that a stopping rule for OSEM algorithm might be formulated, which produces reconstructed images very close to the phantom images, in the case of simulation studies. This work not only proposes a specific stopping rule for the OSEM algorithm, but builds up further a methodology according to which the development of a stopping rule would be possible for any kind of PET scanner configuration. The proposed stopping rule depends on the projection data and camera geometry, for which the calculation of the parameters A , a and b of equation (5)

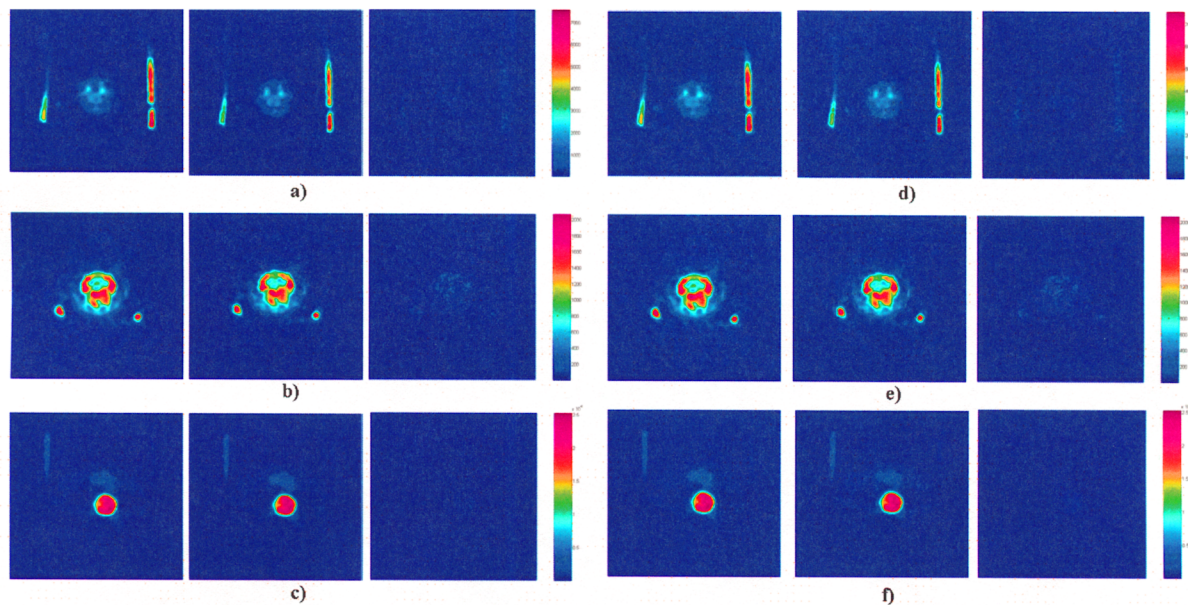


Fig. 6. The validation of stopping rule using the Digimouse slices #16, #33 and #106. The images in left column (a, b and c) have been reconstructed using OSEM with 2 subsets, while the images in right column (d, e and f) have been reconstructed using OSEM with 4 subsets. In each set from right to left the images are: phantom image, reconstructed image and difference between them. A red-green-blue color map used, so that the differences between phantom and reconstructed images can be viewable.

need to be calculated. The present study has been done for two and four subsets. Further study is needed to see how the stopping rule parameters A , a and b , depend on the number of subsets. In addition, it is necessary to find out whether the stopping rule is affected by different image topologies or not. Finally, the effect of noise coming from absorption and scattering must be examined.

REFERENCES

- [1] G. Kontaxakis, "Positron Emission Tomography," in : *Encyclopedia of Medical Devices and Instrumentation, 2nd edition*, Vol. 5, pp. 406-418, John Wiley & Sons, Hoboken, New Jersey, 2006.
- [2] L.A. Shepp, Y.Vardi, "Maximum Likelihood Reconstruction for Emission Tomography," *IEEE Trans Med Imag*, 1(2): 113-121, 1982.
- [3] M. Hudson, R. S. Larkin, "Accelerated Image Reconstruction using Ordered Subsets of Projection Data," *IEEE Trans. Med. Imag.* 13: 601-609, 1994.
- [4] D. W. Townsend, "Physical Principles and Technology of Clinical PET Imaging," *Ann Acad Med Singapore*, 33(2): 133-145, 2004.
- [5] Veklerov E., Llacer J., "Stopping Rule for the MLE Algorithm Based on Statistical Hypothesis Testing", *IEEE Trans. Med. Imag.*, Vol MI-6, No 4, 1987.
- [6] Bissantz N., Mair B. A. and Munk A., "A multi-scale stopping criterion for MLEM reconstructions in PET", *IEEE Medical Imaging Conference*, San Diego, October 29 – November 4 2006, USA.
- [7] G. Kontaxakis, G. Tzanakos, "A stopping criterion for the iterative EM-MLE image reconstruction for PET," *SPIE. Medical Imaging 1996: Image Processing*, M. H. Loew, K.M. Hanson, Eds., vol. 2710: 133-144, February 1996.
- [8] A. Gaitanis, G. Kontaxakis, G. Panayiotakis, G. Spyrou, G. Tzanakos, "The role of the updating coefficient of the ML-EM algorithm in PET image reconstruction," *Eur. J. Nucl. Med Mol. Imag.*, 33 (Suppl. 2):314, 2006.
- [9] A. Gaitanis, G. Kontaxakis, G. Spyrou, G. Panayiotakis, G. Tzanakos, "PET image reconstruction: A stopping rule for the MLEM algorithm based on properties of the updating coefficients",

UA/PHYS/PET/27-4-2008/

UA/PHYS/PET/9-11-2008/

(unpublished).

- [10] E. J. Hoffman, P. D. Cutler, W. M. Digby, J. C. Mazziotta, "3D phantom to simulate cerebral blood flow and metabolic images for PET," *IEEE Trans. on Nuclear Science*, NS-37(2): 616-620, 1990.
- [11] Dodgas B., Stout D., Chatziioannou A. F. and Leahy R. M., Digimouse: a 3D whole body mouse atlas from CT and cryosection data, *Phys. Med. Biol.* 52(2007), 577-587.